Available online at www.sciencedirect.com
SCIENCE DIRECT®
Journal of Membrane Science 239 (2004) 39–53
journal of MEMBRANE SCIENCE
www.elsevier.com/locate/memsci

Flux decline during nanofiltration of naturally-occurring dissolved organic matter: effects of osmotic pressure, membrane permeability, and cake formation

James E. Kilduff [a,*], Supatpong Mattaraj [a], Georges Belfort [b]

[a] *Department of Civil and Environmental Engineering, Rensselaer Polytechnic Institute, 110 8th Street/317 MRC Building, Troy, NY 12180, USA*
[b] *Isermann Department of Chemical Engineering, Rensselaer Polytechnic Institute, 110 8th Street/Rickets Building, Troy, NY 12180, USA*

Received 17 April 2003; received in revised form 19 December 2003; accepted 30 December 2003

Available online 6 May 2004

Abstract

Nanofiltration of naturally-occurring dissolved organic matter (NOM) by an aromatic polyamide membrane was measured in a crossflow bench-scale test cell and modeled using a semi-empirical osmotic pressure/cake formation model. Our objective was to examine flux decline due to NOM fouling while explicitly accounting for flux decline due to osmotic effects and changes in membrane permeability. This approach allowed quantification of the effect of ionic composition on specific NOM cake resistance, and yielded insight into flux decline due to enhanced NaCl rejection by the NOM deposit. In the absence of NOM, increasing NaCl concentration reduced salt rejection and decreased membrane permeability. Flux decline was modeled by accounting for changes in osmotic pressure with time, and by employing an effective permeability. The addition of calcium significantly reduced rejection of sodium and feed conductivity, and thus mitigated flux decline. Increasing pH from 4 (near membrane pI) to 10 increased the effective permeability but also increased NaCl rejection, which resulted in greater flux decline. The presence of NOM caused greater flux decline resulting from a combination of NOM cake resistance and increased rejection of NaCl by negatively charged NOM functional groups. Increasing NaCl concentration had little effect on the mass of NOM deposited, but significantly increased the specific resistance of the NOM cake. The effect of ionic strength on specific resistance correlated with a reduction in NOM size, estimated by separate UF permeation experiments and size exclusion chromatography analysis of UF permeate. Therefore, increased specific cake resistance is consistent with a more compact, less porous cake. Flux decline by NOM solutions showed a maximum at pH 7, where salt rejection was also a maximum. Binding of calcium reduced the ability of NOM to enhance NaCl rejection, and likely increased NOM cake resistance. Flux decline caused by NOM fouling in the presence of calcium was only significantly different than that caused by NOM in a solution of NaCl at the same ionic strength when the calcium concentration corresponded to saturation of NOM binding sites.

Keywords: Nanofiltration; Fouling; Natural organic matter; Water treatment; Concentration polarization

1. Introduction

The use of membrane filtration as a drinking water treatment technology has increased in recent years, motivated in part by more stringent drinking water regulations [1]. Nanofiltration (NF), one of several alternative membrane filtration technologies, has been used to remove divalent cations and natural organic matter (NOM) from surface waters [2]. The removal of NOM has been motivated to control color, and in many cases, reduce the concentrations of halo-methanes and halo-acetic acids that form when NOM-containing water is disinfected with chlorine [3–5]. NF is a pressure-driven membrane process combining Donnan exclusion and sieving separation mechanisms. NF processes operate at pressures between 350 and 1000 kPa—much lower than reverse osmosis (RO) (1400–6800 kPa), but higher than ultrafiltration (UF) (<70 to 500 kPa). The molecular weight cut-off (MWCO) is generally between 300 and 1000 Da [6]. Rejection of monovalent ions by NF membranes is typically on the order of 70%,

* Corresponding author. Tel.: +1-518-276-2042; fax: +1-518-276-3055.
E-mail address: kilduff@rpi.edu (J.E. Kilduff).

0376-7388/$ – see front matter © 2004 Elsevier B.V. All rights reserved.
doi:10.1016/j.memsci.2003.12.030

while rejection of color, organic carbon, and trihalomethane precursors can be much higher, generally between 90 and 95%. Rejection of hardness ions in membrane softening applications generally ranges from 85 to 95% [7–10].

A limitation of more widespread application of membrane processes is the marked decrease in membrane performance that occurs during potable water treatment as a result of fouling [11]. Membrane fouling can be caused by the accumulation of rejected inorganic and organic species, and by biological activity; it reduces membrane performance, increases operating costs, and shortens membrane life [1]. Natural organic matter is considered a major cause of NF fouling during filtration of surface waters [5,12–18]. While the mechanisms of fouling by NOM have been the subject of increased study, they are still not well understood, in part because NOM occurs naturally as heterogeneous mixtures, with properties that can vary geographically, and temporally for a single location.

Membrane fouling in the presence of NOM can be influenced by (1) membrane characteristics, including pore size, water permeability, charge, and surface chemical properties [17,19]; (2) feed solution composition including ionic strength, hardness ion concentrations, and pH [15,17,20,21]; (3) NOM properties, including molecular weight and polarity [13,15,20]; and, (4) hydrodynamic and operating conditions including initial solution flux, crossflow velocity, recovery, and the mass transfer properties of the fluid boundary layer [15,16,22]. In this paper we focus on effects of solution composition, with an emphasis on ionic composition.

Many of the overall impacts of ionic composition (pH, ion concentration, ion valence) on fouling by natural organic matter have been identified in previous studies [14,15,23–25]. Through charge screening, ion pair formation, and complexation, ions in solution can influence the solubility, configuration, and fouling potential of NOM. However, ion composition also influences flux decline through the development of osmotic pressure, and for charged membranes, by affecting ion rejection through Donnan exclusion [26]. In addition, increases in ion concentration can reduce the permeability of charged membranes [26–28]. Few investigations have attempted to distinguish the flux decline due to NOM fouling from flux decline due to osmotic effects and changes in membrane permeability in a quantitative way.

A methodology employing a semi-empirical model to describe permeate flux as a function of time is proposed as an approach to isolate the impact of NOM in terms of both the specific resistance of NOM deposits and the effect of NOM on salt rejection. This approach requires an assessment of how the ionic composition of the feed solution affects membrane performance in the absence of NOM, in terms of both osmotic effects and changes in membrane permeability. To support these objectives, permeate flux and solute rejection were first measured using salt solutions in the absence of NOM, and then using mixtures of salts and NOM.

2. Experimental

2.1. NOM isolation and characterization

Dissolved naturally occurring organic matter (NOM) was isolated from the Tomhannock Reservoir (TMK), a drinking water source for Troy, NY. NOM was quantified as dissolved organic carbon (DOC); the DOC of TMK water averaged about $3\,\mathrm{mg\,C\,l^{-1}}$. The Tomhannock watershed consists of upland forest and mixed agricultural/residential development. NOM was isolated using a field reverse osmosis system following the approach described previously [29,30]. NOM was pretreated using a 5 μm prefilter, a sodium-form cation exchange softener, and two virgin polypropylene cartridge filters (1 and 0.45 μm) in series. The isolated NOM was kept in refrigerator at 4 °C before analysis and sample preparation.

Molecular weight and polydispersity were measured using high-pressure size exclusion chromatography (HPSEC) as described previously [31,32]. The HPSEC instrumentation (Hewlett-Packard 1100, Palo Alto, CA) included a Waters Protein-Pak 125 modified silica column and variable wavelength UV detector. Benzoic acid and poly(styrene sulfonate) were used as standards.

The aquatic humic substance (humic and fulvic acids) content of NOM was quantified by applying NOM concentrates to a methyl methacrylate resin bed (Supelite DAX-8, Supelco, St. Louis, MO) at pH 2 employing a capacity factor (assuming frontal chromatography and neglecting mass transfer limitations) of 100 [33]. The adsorbed fraction, designated “hydrophobic” humic substances (HPO), was subsequently back-eluted from the column using a pH 11 solution while the non-retained fraction was designated “hydrophilic” organic acids (HPL) [34]. Early work on humic substance adsorption by synthetic resins established that adsorption was dominated by hydrophobic interactions [35]. Aiken et al. [36] compared several resins and identified the poly(methyle methacrylate) XAD 8 as having good sorption properties (rate, capacity, and reversibility) for humic substances. This resin is of relatively low polarity with low ion exchange capacity on the order of $10^{-2}\,\mathrm{meq.\,g^{-1}}$ resin. Preparative isolation and fractionation schemes have been developed further by U.S.G.S. researchers [37,38]. The resin employed in this work was 40/60-mesh size with a mean surface area $160\,\mathrm{m^2\,g^{-1}}$ and a mean pore diameter of 225 Å. As-received resin was first washed in 0.1 M NaOH solution, then sequentially soxhlet extracted using acetone and methanol for 24 h each, and exhaustively rinsed with reagent grade I water.

Acidic functional groups in the NOM structure can play an important role in membrane processes due to electrostatic interactions with the membrane surface. The two major acidic functional groups are carboxylic groups, which are considered to be significantly ionized at pH values >6, and the phenolic groups, which are predominantly un-ionized at pH values <8 [39,40]. Proton dissociation of organic acid

components of NOM (organic acidity) was determined by titrating 70-ml NOM samples under positive CO_2-free N_2 pressure with CO_2-free NaOH solutions prepared by diluting concentrated NaOH solutions with CO_2-free (boiled) reagent grade I water. Samples were titrated from an initial pH of 3.00 ± 0.02, to assure protonation of carboxylic groups, to a final pH of 10. Solution pH was measured using an Orion Ross semi-micro combination epoxy body probe and a pH meter (Accumet Model 50, Fisher Scientific). Titrant was delivered to the sample using a Class A, 5 ml microburret, marked at 0.01 ml increments, with a 70 ml integral reservoir (Kimax, Fisher Scientific) which remained closed to the atmosphere except during buret refill. For each incremental change in pH, the moles of base added to an NOM sample in excess of that necessary to effect the same change in pH for water only is attributed to buffering by NOM. Carboxyl groups were assumed to contribute all titratable charge up to pH 7, and phenolic groups were assumed to account for the additional titratable charge to pH 10 [39,41,42]. Oliver et al. [42] report that carboxylic acidity (to pH 7) of aquatic humic substances from nineteen different source waters throughout the United States ranged from 5.1 to 13.4 μeq. mg^{-1} C with an average value of 10.0 and standard deviation of 1.7 μeq. mg^{-1} C.

Binding of calcium by NOM was determined in batch reactors. NOM solutions (10 mg/l DOC, 50 ml) were amended with calcium ion (as $CaCl_2$) to produce total calcium concentrations ranging from 0.0001 to 0.01 M. Reactors were mixed completely for 4 h, a time sufficient to assure equilibrium based on constant free calcium concentrations. Free (non-complexed) calcium was measured using an ion-specific electrode (Thermo Orion) and a pH/ISE meter (Accumet Model 50, Fisher Scientific) calibrated with external standards. The complexed calcium was calculated by difference. Precision of such measurements (relative standard deviation) was within 5% except for the data corresponding to the lowest calcium concentration, for which the R.S.D. was within 14%.

2.2. NF characterization

An aromatic polyamide thin-film composite membrane (NF-70, Dow-FilmTec Inc., Minneapolis, MN) was chosen for this research as representative of a class of membranes used increasingly in water treatment applications. The thin-film composite NF-70 membrane has an isoelectric point near pH 4 [43,44] and a surface charge of about −25 mV at pH 7 with a background electrolyte of 0.01 M NaCl [44]. Vrijenhoek et al. [44] report an average roughness of 43.3 nm, defined as the average deviation of peaks and valleys from the mean plane, i.e., the average of all height values obtained by AFM analysis. A molecular weight cut-off of about 200 Da has been reported for this membrane [45], and contact angle of $28 \pm 2^\circ$ was measured using the captive bubble technique. The salt (NaCl) rejection is about 70% [9] and the magnesium sulfate rejection is 95%, as reported by the manufacturer (conditions: 2000 mg l^{-1} $MgSO_4$, 70 psi (483 kPa), and 25 °C).

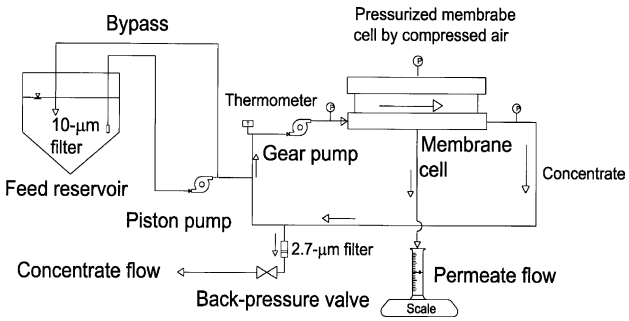

Fig. 1. Schematic diagram of the nanofiltration system.

Membrane sheets were cleaned and pre-compacted at 400 kPa using tap water treated with a mixed bed ion-exchanger and activated carbon (DI water). After membrane compaction (indicated by a steady-state flux), DI water was used to determine the clean water permeability (L_p), which averaged $3.36 \pm 0.28 \times 10^{-8}$ m s^{-1} kPa (0.121 LMH kPa^{-1}) at 23 °C. Membrane sheets were stored in 1% sodium *meta*-bisulfite ($Na_2S_2O_5$) at 4 °C to prevent microbial activity and oxidation.

2.3. Crossflow bench-scale test cell

Solution flux experiments were conducted using the cross-flow bench scale membrane test system depicted schematically in Fig. 1. Additional details of this system were described by Allgeier and Summers [46]. This system consists of a stainless steel cell (SEPA, Osmonics Inc. Minnetonka, MN), a high-pressure stainless-steel piston feed pump, and a high capacity booster (gear) pump to maintain high flow rates in a recycle loop. A 155 cm^2 (24 in.^{2}) membrane sheet and a feed channel spacer (0.086 cm high with three to four strands per cm) were mounted between halves of the stainless steel cell, and were sealed with an o-ring. A flowrate, Q, of 530 ml min^{-1} was maintained in the recycle loop (independent of the feed flow rate and recovery). A crossflow velocity of 0.1 m s^{-1} was estimated based on a cell cross-sectional area, A_f, of 1.23×10^{-4} m^2 and a spacer-filled porosity, ε, of 0.72 computed as described by Da Costa et al. [47]. A Reynolds number (N_{Re}) of approximately 104 was computed on the basis of the hydraulic diameter. Recovery was maintained at 85%, and inlet temperature was approximately 23 °C during filtration experiments.

2.4. Flux experiments

NOM-free reagent-grade sodium chloride solutions (concentrations ranging from 0.004 to 0.10 M) were used to evaluate the effects of salt concentration polarization. The effects of fouling by NOM were evaluated using feed solutions containing 10 mg C l^{-1}. Solution pH was

adjusted to pH 7, and ionic strength was adjusted to 0.01 M as NaCl (i.e., corresponding to a conductivity of 1070 $\mu S\,cm^{-1}$ at 25 °C). Prior to filtration, the membrane system was flushed with feed solution. The initial solution flux was subsequently adjusted to $1.25 \times 10^{-5}\,m\,s^{-1}$ ($45\,L\,m^{-2}\,h^{-1}$) while the transmembrane pressure was kept constant during filtration. Permeate flow was continuously measured throughout the filtration run. Permeate and retentate flows were monitored using an analytical balance (Model TR-4102, Denver Instrument Co., Arvada, CO). Permeate and retentate (bleed) flows were periodically sampled to calculate rejection and mass balance.

2.5. Analytical methods

NOM concentrations were measured as dissolved, non-purgeable carbon using a carbon analyzer (Model 1010, OI Analytical, College Station, TX) employing high temperature wet oxidation. External standards (ranging from 0 to 10 $mg\,l^{-1}$ DOC) were prepared using potassium hydrogen phthalate in reagent grade (Milli-Q) water, which was also used as a blank. UV absorbance was measured using a diode-array spectrophotometer (HP8452A, Hewlett Packard, Menlo Park, CA). Sodium and calcium concentrations were measured by atomic absorbance (AA) spectrometry (AAnalyst 300, Perkin Elmer Corp., Norwalk, CT). External calibration curves were prepared using reagent-grade NaCl and $CaCl_2$. Measurements of pH, conductivity, and temperature were made using an Advanced Portable Meter (AP50, Denver Instrument Co., Arvada, CO). Ionic strength of samples was calculated using a correlation between conductivity and ionic strength of NaCl standards, I.S. $[M] = 0.5 \sum C_i Z_i^2 = 9.5 \times 10^{-6} \times (\mu S\,cm^{-1})$. Hardness and alkalinity were determined using titration techniques as described in *Standard Methods* [48].

2.6. Ultrafiltration experiments

The membrane permeation of NOM in a cross-flow, hollow-fiber ultrafiltration system (AG Technologies, Needham, MA) was measured to determine the effects of ionic strength on NOM permeation, following the protocol described by Kilduff and Weber [49]. These experiments were done to evaluate changes in NOM size that result from changes in ionic strength. The UF membrane used in this study had a 5 kDa molecular weight cut-off, calibrated by the manufacturer using poly(vinylpyrrolidone). The system was operated in a recycle mode using a high recycle flow to maintain well-mixed conditions, minimize fouling, and reduce concentration polarization. The NOM concentration in the feed reservoir is given by the integrated mass balance equation assuming completely mixed conditions [49,50]:

$$C_{feed} = C_{feed,0}\left[\frac{V_0}{V_0 - V_{perm}}\right]^{\mathcal{R}} \quad (1)$$

where V_0 is the initial solution volume (l); $C_{feed,0}$ the initial feed concentration of NOM components capable of passing the membrane, and V_{perm} the cumulative permeate volume. The model was fitted to filtration data either by varying rejection, $\mathcal{R}$ ($\mathcal{R} = 1 - C_{permeate}/C_{feed}$) to minimize the sum of squared residuals between the data and the model fit, or by linear regression of the log-transformed form of Eq. (1).

3. Theory

3.1. Solution flux

Flux of solutions containing salt (e.g., NaCl) is given by:

$$J_v = L_p(\Delta P - \sigma\,\Delta\pi) = \frac{\Delta P - \sigma\,\Delta\pi}{\mu(R_m + R_{non\text{-}rec})} \quad (2)$$

where L_p is the membrane permeability ($m\,s^{-1}\,kPa^{-1}$); ΔP the average transmembrane pressure (kPa); σ the osmotic reflection coefficient, and $\Delta\pi$ the difference in osmotic pressure between the membrane and permeate stream, $\Delta\pi = \pi_{mem} - \pi_{perm}$ (kPa). The reflection coefficient was estimated by the intrinsic membrane rejection, $\mathcal{R}_{mem}$, where $\mathcal{R}_{mem} = 1 - C_{perm}/C_{mem}$; C_{perm} and C_{mem} are the concentrations in the permeate and at the membrane surface, respectively. The solution flux can also be written in terms of membrane resistances, where R_m is the membrane hydraulic resistance (m^{-1}); $R_{non\text{-}rec}$ the any non-recoverable resistance that develops during filtration (m^{-1}); and μ the dynamic viscosity of the solution ($kg\,m^{-1}\,s^{-1}$).

Under constant-pressure operation, assuming constant membrane permeability, and in the absence of feed components that cause fouling by pore blockage or cake formation (e.g., NOM), the change in solution flux is related to the change in osmotic pressure as a result of solute (e.g., NaCl) accumulation at the membrane-solution interface. The osmotic pressure is correlated with NaCl concentration, with π (kPa) $= \alpha C$ ($mol\,l^{-1}$), where $\alpha = 4815$ ($kPa\,l\,mol^{-1}$) at 25 °C under the ideal solution assumption [51]. Therefore, $\Delta\pi = \alpha(C_{mem} - C_{perm})$. Using the intrinsic rejection this can be written $\Delta\pi = \alpha\mathcal{R}_{mem}C_{mem}$. The concentration at the membrane surface was eliminated in favor of C_{reten}, the directly measurable bulk (retentate recycle loop) concentration, as follows. First, clean water flux (J_0) experiments were conducted in the absence of NaCl to obtain values for R_m (using Eq. (2) written in terms of resistances with $\sigma\,\Delta\pi = 0$ and $R_{non\text{-}rec} = 0$). The additional fouling resistance $R_{non\text{-}rec}$ was measured by a second clean water flux measurement following filtration of a salt solution and subsequent membrane cleaning (using Eq. (2) with $\sigma\,\Delta\pi = 0$). Solution flux in the presence of salt was then measured under steady-state conditions with different salt concentrations. Data from such experiments, shown in Fig. 2, were used to calculate $\sigma\,\Delta\pi$ using Eq. (2) and C_{mem} using $\sigma\,\Delta\pi = \sigma\alpha(C_{mem} - C_{perm})$. The ratio $\beta = C_{mem}/C_{reten}$ was correlated as a function of NaCl concentration, and the

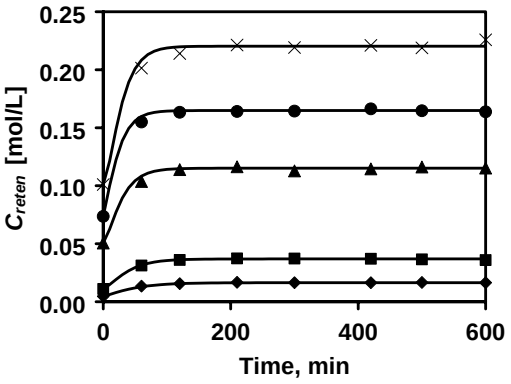

Fig. 2. Salt concentration in the retentate stream; symbols are experimental data, lines are mass balance model fits. All solutions were NOM-free. NaCl concentrations: (◆) 0.004 M; (■) 0.01 M; (▲) 0.05 M; (●) 0.075 M; (×) 0.10 M. Operating conditions: initial solution flux $= 1.25 \times 10^{-5}\,\mathrm{m\,s^{-1}}$, crossflow velocity $= 0.1\,\mathrm{m\,s^{-1}}$, recovery $= 0.85$, and $T = 23\,^{\circ}\mathrm{C}$.

osmotic pressure difference was then written in terms of C_{reten}, $\Delta\pi = \alpha\beta\mathcal{R}_{\mathrm{mem}}C_{\mathrm{reten}}$. Taking the time derivative of Eq. (2) yields:

$$\frac{\mathrm{d}J_{\mathrm{v}}}{\mathrm{d}t} = -\frac{\sigma\alpha\mathcal{R}_{\mathrm{mem}}\beta}{\mu(R_{\mathrm{m}} + R_{\text{non-rec}})}\left(\frac{\mathrm{d}C_{\mathrm{reten}}}{\mathrm{d}t}\right) \tag{3}$$

3.2. Overall system mass balance

The time rate of change of C_{reten} was described using an overall material balance on the bench-scale test cell and recycle loop. The cell was operated using a high recycle flow rate, which warranted treatment of the system as a completely mixed flow reactor (CSTR):

$$V_{\mathrm{sys}}\frac{\mathrm{d}C_{\mathrm{reten}}}{\mathrm{d}t} = Q_{\mathrm{feed}}C_{\mathrm{feed}} - Q_{\mathrm{reten}}C_{\mathrm{reten}} - Q_{\mathrm{perm}}C_{\mathrm{perm}} - k_{\mathrm{l}}a_{\mathrm{s}}(C_{\mathrm{ss}} - C_{\mathrm{reten}})V_{\mathrm{sys}} \tag{4}$$

where V_{sys} is the recirculating volume (about 70 ml); flow, Q, and concentration, C, are subscripted to indicate either the feed stream (*feed*), retentate recycle loop (*reten*) or permeate (*perm*). If all flows remain constant, this system reaches a steady-state condition. The last term accounts for mass transfer from the bulk to the membrane surface, forming the concentration polarization layer, which occurs before steady state is reached. This mass transport is approximated by a linear driving force, where C_{ss} is the steady-state NaCl concentration in the retentate stream ($\mathrm{mol\,m^{-3}}$), k_{l} is a mass transfer coefficient ($\mathrm{m\,s^{-1}}$), and a_{s} is the volumetric specific surface area ($\mathrm{m^2\,m^{-3}}$) equal to the effective membrane surface area divided by the recycle loop volume; $a_s \approx 220.8$ ($\mathrm{m^2\,m^{-3}}$). This term goes to zero when the system reaches steady state and $C_{\mathrm{reten}} = C_{\mathrm{ss}}$. The product $k_{\mathrm{l}}a_{\mathrm{s}}$, considered an "overall" mass transfer coefficient, was estimated by fitting the material balance model to measured C_{reten} values as a function of time, as shown in Fig. 2. Using a fourth-order Runge–Kutta routine, the overall mass transfer coefficient was varied to minimize the sum of squared residuals (SSR) for each feed salt concentration. Parameter search was done using an optimization scheme based on a generalized reduced gradient (GRG) non-linear programming algorithm, implemented in a commercial software package (Microsoft Excel). Forward differencing was used to estimate partial derivatives of the objective and constraint functions. Convergence was determined when relative changes in fitted parameters were less than 0.0001 for five successive iterations.

3.3. Cake formation model

A good deal of evidence has been presented in the literature to suggest that cake formation predominates as a mode of fouling by NOM solutions [12,15,16,19,25,52]. This model has been described previously in the literature [53–55]. The deposition of solute molecules on the membrane surface provides an additional resistance, R_{c}, to solution flux:

$$J_{\mathrm{v}} = \frac{\Delta P - \sigma\,\Delta\pi}{\mu(R_{\mathrm{m}} + R_{\text{non-rec}} + R_{\mathrm{c}})} \tag{5}$$

When the feed solution contains both salt and NOM, the change in solution flux is related to the change in osmotic pressure as a result of concentration polarization (assumed to be primarily caused by salt), and the change in the hydraulic resistance of the NOM cake that forms on the membrane surface:

$$\frac{\mathrm{d}J_{\mathrm{v}}}{\mathrm{d}t} = -\frac{\sigma_{\mathrm{s}}\alpha_{\mathrm{s}}\mathcal{R}_{\mathrm{mem}}\beta_{\mathrm{s}}}{\mu(R_{\mathrm{m}} + R_{\text{non-rec}} + R_{\mathrm{c}})}\left(\frac{\mathrm{d}C_{\mathrm{reten,s}}}{\mathrm{d}t}\right) - \frac{J_{\mathrm{v}}}{R_{\mathrm{m}} + R_{\text{non-rec}} + R_c}\left(\frac{\mathrm{d}R_{\mathrm{c}}}{\mathrm{d}t}\right) \tag{6}$$

where the subscript *s* refers to NaCl (salt). In the cake formation model, the time rate of change in cake resistance is assumed to be proportional to the rate of change in cake mass, m_{cake} (kg), which increases at a rate proportional to the net rate of convective mass transport toward the membrane surface:

$$\frac{\mathrm{d}R_c}{\mathrm{d}t} = \alpha_{\mathrm{cake}}\frac{1}{A_m}\frac{\mathrm{d}m_{\mathrm{cake}}}{\mathrm{d}t} = \alpha_{\mathrm{cake}}C_{\mathrm{reten,NOM}}(t)(J_v - J^*) \tag{7}$$

where α_{cake} is the specific cake resistance (assumed constant) ($\mathrm{m\,kg^{-1}}$), $C_{\mathrm{reten,NOM}}$ is the NOM concentration in the retentate recycle loop ($\mathrm{kg\,m^{-3}}$), and J^* ($\mathrm{m\,s^{-1}}$) is the effective flux associated with back-transport resulting from crossflow. The development of cake resistance as a function of time, R_{c} in Eq. (6), was evaluated by integrating Eq. (7), and the change in salt concentration, $\mathrm{d}C_{\mathrm{reten,s}}/\mathrm{d}t$, was determined using the overall material balance model, Eq. (4). Eqs. (6) and (7) were integrated using a fourth-order Runge–Kutta routine, using the specific cake resistance and the effective back-transport flux (J^*) as fitting parameters, determined by minimizing the sum of squared residuals (SSR) between the observed and fitted solution flux. Parameter search was done as described in Section 3.2.

4. Results and discussion

4.1. Overall system mass balance

The concentration of NaCl in the retentate stream of the bench scale system (in NOM-free solutions) as a function of time is shown in Fig. 2. Excellent fits of C_{reten} were obtained using Eq. (4) with the overall mass transfer coefficient as the sole fitting parameter. The measured steady state concentration, C_{ss}, the fitted overall mass transfer coefficient, $k_l a_s$, and the calculated value of k_l using $a_s = 220.8$ ($m^2\,m^{-3}$) for each run are tabulated in Table 1. The product $k_l a_s$ was determined with an approximate 95% confidence interval within ±1% of the stated value. The average value of the estimated mass transfer coefficient, $1.6 \times 10^{-5}\,m\,s^{-1}$, is within 13% of the value predicted by the Graetz–Leveque equation, and within 20% of the value predicted by a correlation reported by DaCosta et al. [56] for their 80 MIL-2 spacer, although the Schmidt number, N_{Sc}, employed in that study was much higher than ours. The value predicted using a correlation reported by Schock and Miguel [57] for spiral wound RO applications is about 78% higher than that found here, possibly because their correlation used exponents on N_{Re} and N_{Sc} characteristic of turbulent flow, which was not the case here. Steady state retentate concentrations increased in a roughly linear manner proportional to feed concentration, while the overall mass transfer coefficients declined slightly with increased feed salt concentration.

4.2. Effects of NaCl concentration on flux decline

The measured change in C_{reten} as a function of time was employed in Eq. (3) in an attempt to *predict* the effects of osmotic pressure on flux decline; such effects are illustrated by the data (shown as symbols) in Fig. 3. The model tended to under-predict flux decline; however, the data could be fitted after multiplying the right hand side of Eq. (3) by a constant factor, η:

$$\frac{dJ_v}{dt} = -\eta \frac{\sigma\alpha\mathcal{R}_{mem}\beta}{\mu(R_m + R_{non\text{-}rec})}\left(\frac{dC_{reten}}{dt}\right) \quad (8)$$

Because the parameters σ, α, β, and $\mathcal{R}_{mem}$ were determined independently, the factor η multiplies the clean water permeability, L_p:

$$\eta \frac{1}{\mu(R_m + R_{non\text{-}rec})} = \eta L_p = L_{p,s} \quad (9)$$

Therefore, we interpret η as a permeability reduction factor, with the product ηL_p representing an effective permeability in the presence of salt, $L_{p,s}$. This is equivalent to defining a membrane resistance in the presence of salt, $R_{m,s}$, where $L_{p,s} = 1/(\mu(R_{m,s} + R_{non\text{-}rec}))$ and

$$R_{m,s} = \frac{R_m + (1-\eta)R_{non\text{-}rec}}{\eta} = \frac{1 - \mu R_{non\text{-}rec} L_{p,s}}{\mu L_{p,s}} \quad (10)$$

The effective permeability, $L_{p,s}$ was evaluated by fitting Eq. (8) to the experimental data shown in Fig. 3 using a Fourth-order Runge–Kutta routine, minimizing the sum of squared residuals (SSR) for each feed salt concentration, as described in Section 3.2.

The observation that membrane permeability was reduced in the presence of salt implies that osmotic pressure was overestimated when steady-state NaCl solution flux data were analyzed using Eq. (2) in conjunction with R_m. Hence, values of C_{mem} and β were also overestimated. Therefore, to obtain more accurate estimates of model parameters, an iterative approach was required. Fitted values of effective permeability were used to obtain new estimates of osmotic pressure, C_{mem} and β. These were used with Eq. (8) to generate new estimates of effective permeability. These calculations were repeated until convergence (parameter value changed by less than 1%), generally achieved in less than seven iterations.

Table 1
Overall mass balance model fitting parameters

Parameter	NaCl concentration (M)				
	0.004	0.01	0.05	0.075	0.1
C_{ss} (M)	0.016	0.037	0.114	0.164	0.220
$k_l a_s$ (min^{-1})[a]	0.224	0.218	0.209	0.203	0.207
k_l ($m\,s^{-1}$) $\times 10^5$[b]	1.69	1.65	1.58	1.53	1.56
Average k_l	$1.60 \times 10^{-5}\,m\,s^{-1}$				

[a] The product $k_l a_s$ is the fitted overall mass transfer coefficient, where a_s is the volumetric specific surface area ($m^2\,m^{-3}$) equal to the effective membrane surface area divided by the reactor (recycle loop) volume. The product $k_l a_s$ was determined with an approximate 95% confidence interval within ±1% of the stated value.

[b] k_l is the calculated mass transfer coefficient calculated using $a_s \approx 220.8$ ($m^2\,m^{-3}$).

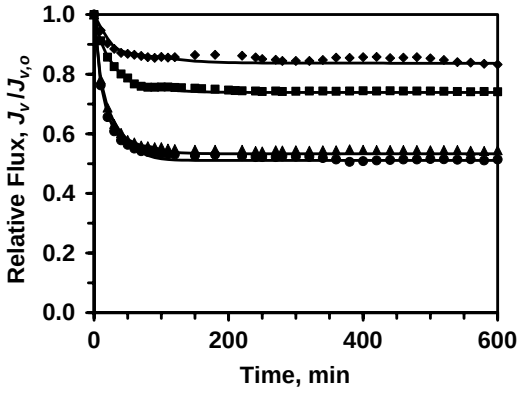

Fig. 3. Effect of salt concentration on solution flux; symbols are experimental data, lines are model fits. NaCl concentrations: (◆) 0.004 M; (■) 0.01 M; (▲) 0.05 M; (●) 0.075 M. Operating conditions: initial solution flux $= 1.25 \times 10^{-5}\,m\,s^{-1}$, crossflow velocity $= 0.1\,m\,s^{-1}$, recovery = 0.85, and temperature = 23 °C.

Table 2
Model and process performance parameters, NaCl feed, effect of NaCl concentration

Parameters[a]	Salt concentration as NaCl[b] (M)				
	0.004	0.01	0.05	0.075	0.1
ΔP (kPa)	408 (59.3 psi)	519 (75.3 psi)	670 (97.3 psi)	881 (127.8 psi)	1172 (170 psi)
$\sigma\,\Delta\pi$ (kPa)	93 (13.4 psi)	186 (26.9 psi)	414 (60.1 psi)	560 (81.2 psi)	723 (104 psi)
$\Delta P - \sigma\,\Delta\pi$ (kPa)	315 (45.9 psi)	333 (48.4 psi)	256 (37.2 psi)	321 (46.6 psi)	449 (66 psi)
J_v ($m\,s^{-1}$) $\times 10^6$	10.8	9.26	6.80	6.45	6.19
C_{mem} (M)	0.024	0.050	0.153	0.214	0.286
C_{reten} (M)	0.016	0.037	0.114	0.164	0.220
C_{perm} (M)	0.002	0.006	0.038	0.056	0.079
$\beta = C_{mem}/C_{reten}$	1.45	1.36	1.33	1.30	1.30
η[c]	0.96	0.76	0.71	0.55	0.52
ηL_p ($m\,s^{-1}\,kPa$) $\times 10^8$	3.43	2.78	2.66	2.01	1.38
$\mathcal{R}_{feed}$ (%)[d]	48.9	46.3	24.7	23.3	22.0
$\mathcal{R}_{reten}$ (%)[e]	85.3	83.8	66.8	65.7	64.2
$\mathcal{R}_{mem}$ (%)[f]	90.0	88.0	75.1	73.7	72.5

[a] Average membrane permeability (L_p) was $3.36 \pm 0.28 \times 10^{-8}\,m\,s^{-1}\,kPa^{-1}$ ($0.121\,LMH\,kPa^{-1}$).
[b] Operating conditions: initial solution flux $= 1.25 \times 10^{-5}\,m\,s^{-1}$, crossflow velocity $= 0.1\,m\,s^{-1}$, recovery $= 0.85$, temperature $= 23\,^{\circ}C$.
[c] The permeability reduction factor, η, was determined with an approximate 95% confidence interval within ±4% of the stated value.
[d] $\mathcal{R}_{feed} = 1 - C_{perm}/C_{feed}$; C_{perm} and C_{feed} are the permeate and feed reservoir DOC concentrations, respectively.
[e] $\mathcal{R}_{reten} = 1 - C_{perm}/C_{reten}$; C_{perm} and C_{reten} are the permeate and recycle loop retentate DOC concentrations, respectively.
[f] $\mathcal{R}_{mem} = 1 - C_{perm}/C_{mem}$; C_{perm} and C_{mem} are the permeate and membrane surface DOC concentrations, respectively.

Fig. 3 presents the effect of salt concentration on solution flux; solid lines are model fits to the experimental data, shown as symbols. Directly measured parameters, parameters estimated from steady state experiments, and fitted parameters are tabulated in Table 2. Values of effective permeability (permeability reduction factor, η) were determined with an approximate 95% confidence interval within ±4% of the stated value.

It is observed that the extent and rate of solution flux decline increased with increasing feed concentration. After accounting for osmotic effects the effective permeability (ηL_p) decreased (i.e., the effective hydraulic resistance $R_{m,s} + R_{non\text{-}rec} = 1/\mu\eta L_p$ increased) by almost a factor of two. The observation that membrane permeability was reduced in the presence of salt is consistent with previous reports in the literature [14,27,28]. These reductions have been attributed to changes in the membrane pore size or porosity, due to polymer matrix compaction or shrinking, caused by an increased ion concentration in the membrane matrix and increased screening of charged moieties [14,27]. An alternative explanation postulates an increase in the frictional coefficients inside the membrane [28]. It may be noted that the reduction in effective permeability with increasing ionic strength observed here is in opposition to any electroosmotic effects. Whereas pressure-driven solvent flux is resisted, and effective hydraulic permeability reduced, by counterion flux generated by a streaming potential produced by the fluid flow, the magnitude of this effect decreases with increasing ionic strength–effective permeability would be expected to increase with increasing ionic strength [58].

The intrinsic membrane rejection decreased significantly with increasing feed concentration, from about 90 to 73%. In part, this can be attributed to an increase in the concentration of salt at the membrane surface and an increase in solute flux relative to the solvent flux. However, electrostatic effects may also play a significant role. Increased ion concentration can cause a reduction in the electrical double layer thickness in membrane pores and thus increase the solute partition coefficient, causing a reduction in the rejection of ionic species [55,58]. Decreased rejection of charged solutes by charged membranes with increasing feed ionic strength has been observed by others, and is consistent with ion exclusion by a Donnan mechanism [26–28,59,60].

4.3. Effects of pH on flux decline

To examine the effects of charge screening in more detail, the effects of pH at constant ionic strength were investigated. Ionization of charged moieties with increasing pH will increase fixed charge and intramembrane electrostatic repulsion. A pH range from 4 (pH near the pI) to 10 was investigated, keeping the ionic strength constant with a feed NaCl concentration of 0.01 M. Fig. 4 illustrates the effect of pH on flux decline; the solid lines are model fits using Eq. (8), fitted parameters are tabulated in Table 3. The rate and extent of flux decline increased with increasing pH, even though the effective permeability increased. The permeability reduction factor, η, increased from 0.80 to 0.93, consistent with increased intramembrane electrostatic repulsion (note that changes greater than 0.03 are statistically significant based on approximate 95% confidence intervals). The increased flux decline with pH was caused primarily by an increase in the magnitude of the dC_{reten}/dt term in Eq. (8), resulting from an increase in rejection, R_{mem}. Such an increase is consistent with increased fixed charge, increased electrical double layer thickness

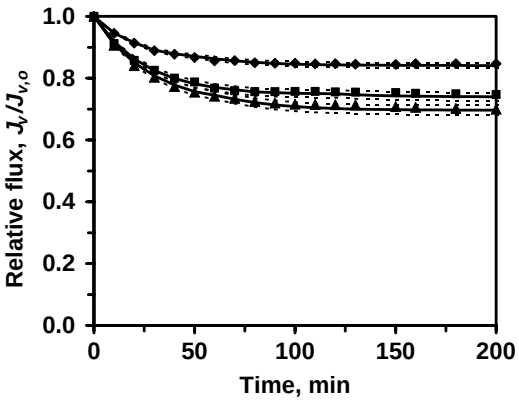

Fig. 4. Effect of pH on solution flux; symbols show experimental data while the solid lines are model fits. Dashed lines show model sensitivity to permeability reduction factors varied +/−5%. Ionic strength = 0.01 M NaCl; pH values: (◆) pH 4 (pH ≈ pI); (■) pH 7; (▲) pH 10. Operating conditions: initial solution flux = 1.25×10^{-5} m s^{-1}, crossflow velocity = 0.1 m s^{-1}, recovery = 0.85, and temperature = 23 °C.

Table 4
Characteristics of Tomhannock (TMK) water

Parameter	Value
Source water	
DOC (mg l^{-1})	2.99
$UV_{254\,nm}$ (cm^{-1})	0.074
SUVA (l mg^{-1} m^{-1})	2.5
Alkalinity (mg l^{-1} $CaCO_3$)	35
Hardness (mg l^{-1} $CaCO_3$)	76
pH	7.2
Isolates	
Molecular weight (Da)[a]	1000
Polydispersity[b]	2.0
%Hydrophobic/%hydrophilic	36.4/63.6
Total acidity (meq. (g DOC)$^{-1}$)	11.2[c] (28.8)[d]

[a] Weight-averaged molecular weight.
[b] Weight-averaged molecular weight/number-averaged molecular weight (M_w/M_n).
[c] Titration from pH 3 to 7.
[d] Titration from pH 3 to 10.

within membrane pores, or both. The concentration at the membrane surface also increased, but not to the same extent that C_{reten} increased; therefore the ratio $\beta = C_{mem}/C_{reten}$ decreased with increasing pH.

The effect of pH on rejection is consistent with the findings of Childress and Elimelech [43] for pH values above the membrane isoelectric point. The results presented here are also consistent with the model invoked by Braghetta et al. [14] to interpret their data. However, in contrast to the findings of this study, they found that solution flux *increased* with increasing pH, as a result of increases in membrane permeability. In their system the effects of membrane permeability, characterized here by η, were more important than the effects of solute rejection. Whereas the value of η also increased with increasing pH in this work, the effects of pH on solute rejection, not membrane permeability, were most important. Possible explanations for these different observations include (1) the larger molecular weight cutoff of the membrane used by Braghetta et al. [14], which was on the order of 1000 Da, as compared to about 200 Da for the membrane in this work; (2) different membrane material and surface charge; or both.

Table 3
Model and process performance parameters, NaCl feed, effect of pH

pH	Parameters				
	η[a]	$\mathcal{R}_{mem}$[b] ($\mathcal{R}_{feed}$)[c]	$J_s = J_v C_p$ (mol m^{-2} h^{-1})	C_{mem}/C_{reten}	J_v (LMH)
4	0.80	0.82 (0.33)	0.29	1.50	38.2
7	0.76	0.88 (0.53)	0.20	1.36	33.5
10	0.93	0.90 (0.57)	0.18	1.20	31.6

[a] The permeability reduction factor, η, was determined with an approximate 95% confidence interval within ±4% of the stated value.
[b] $\mathcal{R}_{mem} = 1 - C_{perm}/C_{mem}$; C_{perm} and C_{mem} are the permeate and membrane surface DOC concentrations, respectively.
[c] $\mathcal{R}_{feed} = 1 - C_{perm}/C_{feed}$; C_{perm} and C_{feed} are the permeate and feed reservoir DOC concentrations, respectively.

4.4. NOM characteristics

The characteristics of the Tomhannock Reservoir NOM, tabulated in Table 4, are representative of many surface water sources in the Northeast US. The organic acidity contributed by carboxylic groups measured by titration from pH 3 to 7 was 11.2 meq. (g DOC)$^{-1}$; this compares to a mean value of 9.1 meq. (g DOC)$^{-1}$ for fulvic acids as reported by Schnitzer [61]. This may contribute, in part, to the predominance of the polar (hydrophilic) components (63.6%) in this water.

4.5. Effect of NOM concentration on NaCl rejection and solution flux

Feed solutions having three different NOM concentrations, 5, 10, and 25 mg DOC l^{-1}, were prepared from TMK isolate. The ionic strength (0.01 M as NaCl) and pH (7) of all feed solutions was the same. Fig. 5 shows the effect of NOM concentration on flux decline. The solid lines represent model fits to Eq. (6); directly measured process parameters and fitted model parameters are tabulated in Table 5. As expected, the presence of NOM caused greater flux decline than solutions of NaCl alone; normalized solution flux (t = 10 h) decreased from 0.74 to 0.35 as NOM concentration increase from 0 to 25 mg l^{-1}. The increased flux decline resulted from a combination of resistance from an NOM deposit and an increased osmotic effect. The osmotic effect increased because the presence of NOM significantly increased NaCl rejection, which can be explained by electrostatic repulsion between Cl^- ions and charged functional groups on the NOM molecules, and which caused an increase in the change of $C_{reten,s}$ with time (Eq. (6)).

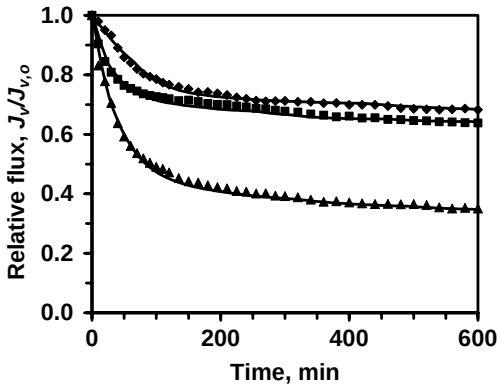

Fig. 5. Effect of NOM concentration on solution flux; symbols show experimental data while the solid lines are model fits. Model fits were calculated after varying the specific resistance parameter ±20%; variations were smaller than the symbols used to represent the data. NOM concentration: (◆) 5 mg l^{-1}; (■) 10 mg l^{-1}; (▲) 25 mg l^{-1}. Operating conditions: initial solution flux = 1.25×10^{-5} m s^{-1}, crossflow velocity = 0.1 m l^{-1}, recovery = 0.85, and temperature = 23 °C.

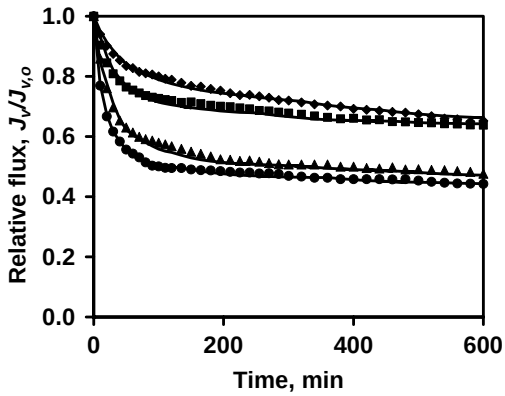

Fig. 6. Effect of ionic strength on NOM solution flux; symbols show experimental data while the solid lines are model fits. Model fits were calculated after varying the specific resistance parameter ±10%; variations were smaller than the symbols used to represent the data. NOM concentration = 10 mg l^{-1}; pH 7. NaCl concentrations: (◆) 0.004 M; (■) 0.01 M; (▲) 0.025 M; (●) 0.05 M. Operating conditions: initial solution flux = 1.25×10^{-5} m s^{-1}, crossflow velocity = 0.1 m s^{-1}, recovery = 0.85, and temperature = 23 °C.

Two factors contributed to an increase in the resistance of the NOM deposit with increasing NOM concentration. First was the mass of NOM deposited, which was 6.5, 10.5 and 39.8 mg for feed solutions concentrations of 5, 10 and 25 mg l^{-1}, respectively. In addition, the specific resistance of the cake increased by a factor of almost two when the NOM concentration was increased from 5 to 10 mg l^{-1}. The increase was statistically significant, because the specific resistance was determined with an approximate 95% confidence interval within ±10% of the stated value. However, the specific resistance appears to have reached a limiting value because further increases were not observed when the NOM concentration was increased to 25 mg l^{-1}. The increase in cake resistance can be explained by a decrease in cake porosity with increasing NOM concentration, possibly resulting from a reconfiguration of NOM molecules to adopt more compact arrangements. (Whereas this would also imply an increase in the cake density, which would have the opposite effect, the specific resistance is more sensitive to changes in porosity.) The sharp decrease in solution flux observed with the 25 mg l^{-1} feed solution appears to be related primarily to an increase in the NOM mass deposited, because the salt rejection and specific resistance of the cake (as judged from a sensitivity analysis on fitted parameters) were not significantly different from the values obtained for the 10 mg l^{-1} solution. Cohen and Probstein [62] observed similar behavior for a colloidal solution of ferric hydroxide, when the colloidal dispersion was unstable, which resulted in rapid aggregation. The relatively constant value of the specific resistance observed may reflect an increased rate or extent of aggregation, and a balance between increases in porosity and decreases in cake density.

4.6. Effect of NaCl concentration in the presence of NOM

Careful examination of the data in Table 5 shows that the trends in specific resistance parallel those in the NaCl rejection. The role of NaCl concentration was further investigated by amending solutions of TMK NOM (10 mg l^{-1}, pH 7) with varying amounts of NaCl to yield a range of ionic strength. Fig. 6 illustrates the effect of ionic strength on

Table 5
Model and process performance parameters, TMK–NOM feed, effect of NOM concentration

Concentration (mg l^{-1})	J/J_0 (10 h)	α_{cake} (m kg^{-1}) $\times 10^{-16}$[a]	J^* (LMH)[b]	$\mathcal{R}_{feed}$[c] %DOC	$\mathcal{R}_{feed}$[c] %conductivity
0	0.74	–	–	–	45.1–50.5 (46.3)
5	0.68	2.15	31.0	96.4–97.5 (97.1)	63.8–72.6 (65.7)
10	0.64	3.93	30.3	97.7–98.4 (97.9)	70.1–79.5 (72.7)
25	0.35	3.62	16.0	97.4–97.9 (97.7)	61.9–75.8 (65.2)

Solution conditions: NOM concentration: varied; ionic strength = 0.01 M as NaCl; pH 7. Operating conditions: initial solution flux = 1.25×10^{-5} m s^{-1}, crossflow velocity = 0.1 m s^{-1}, recovery = 0.85, temperature = 23 °C. The average of seven rejection values is shown in parenthesis.

[a] The specific cake resistance, α_{cake}, was determined with an approximate 95% confidence interval within ±10% of the stated value.

[b] The effective back transport flux, J^*, was determined with an approximate 95% confidence interval within ±2% of the stated value.

[c] $\mathcal{R}_{feed} = 1 - C_{perm}/C_{feed}$; C_{perm} and C_{feed} are the permeate and feed reservoir DOC concentrations or conductivities, respectively.

Table 6
Model and process performance parameters, TMK–NOM feed, effect of ionic strength

I.S. (M)	J/J_0 (10 h)	α_{cake} (m kg) $\times 10^{-16}$[a]	J^* (LMH)[b]	$\mathcal{R}_{feed}$[c] %DOC	$\mathcal{R}_{feed}$ %conductivity[c]
0.004	0.652	1.76	30.6	82.7–86.3 (84.6)	45.1–50.6 (48.1)
0.01	0.638	3.93	30.2	97.7–98.4 (97.9)	70.1–79.5 (72.7)
0.025	0.477	5.24	22.8	93.5–94.6 (94.1)	41.3–50.6 (44.1)
0.05	0.443	5.97	20.4	95.7–96.9 (96.0)	33.4–38.6 (35.5)

Solution conditions: NOM concentration: 10 mg l^{-1}; pH 7. Operating conditions: initial solution flux $= 1.25 \times 10^{-5}$ m s^{-1}, crossflow velocity $= 0.1$ m s^{-1}, recovery $= 0.85$, temperature $= 23\,^{\circ}$C. The average of seven rejection values is shown in parenthesis.

[a] The specific cake resistance, α_{cake}, was determined with an approximate 95% confidence interval within ±10% of the stated value.

[b] The effective back transport flux, J^*, was determined with an approximate 95% confidence interval within ±2% of the stated value.

[c] $\mathcal{R}_{feed} = 1 - C_{perm}/C_{feed}$; C_{perm} and C_{feed} are the permeate and feed reservoir DOC concentrations or conductivities, respectively.

solution flux. The solid lines represent model fits to Eq. (6); directly measured process parameters and fitted model parameters are tabulated in Table 6. Increased ionic strength from 0.004 to 0.05 M NaCl decreased relative solution flux ($t = 10$ h) from 0.65 to 0.44; in all cases flux reductions were significantly greater than in the presence of salt alone. The amount of NOM deposited averaged 12.9 ± 2.5 mg and did not show any significant trend with ionic strength. However, as shown in Fig. 7, increases in flux decline correlate with statistically significant increases in the specific resistance of the cake; this parameter increased by a factor of about three over the range of ionic strength studied. It is likely that the increase in salt concentration in the cake layer reduced charge repulsion between ionized functional groups on single NOM molecules, allowing them to adopt more compact configuration, and between NOM molecules, increasing the compactness of the cake, resulting in lower cake porosity.

A change in NOM configuration with increasing ionic strength is consistent with a model of NOM structure proposed by Ghosh and Schnitzer [63] and has been shown to influence mass transfer in sorption processes [64]. Kilduff and Weber [49] explained the effect of ionic strength on the rejection of humic acid by ultrafiltration membranes in terms of changes in humic acid molecular size. A similar approach was used here provide evidence that increases in specific cake resistance result from changes in NOM configuration and/or size.

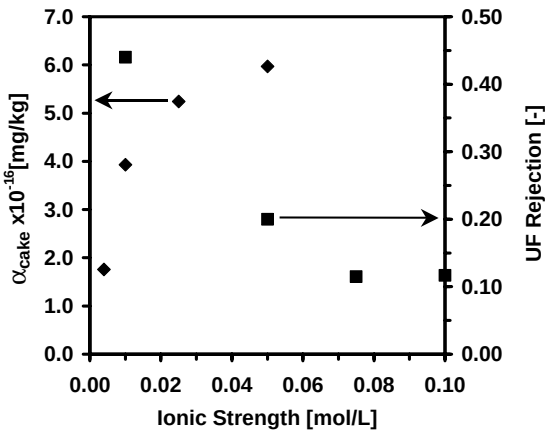

Fig. 7. Effect of ionic strength on the specific resistance of the NOM cake formed in nanofiltration (◆) compared to the effect of ionic strength on feed DOC rejection by UF membrane, a measure of NOM size (■). NOM concentration = 10 mg l^{-1}.

The effect of ionic strength on NOM macromolecular configuration was investigated by measuring transport across a 5 kDa molecular weight cut-off ultrafiltration membrane. The 5 kDa MWCO was selected because it exhibited near zero rejection of salt, thus preventing changes in ionic strength upstream of the membrane during the experiment. Also, a very small fraction of the TMK water was retained on the 5 kDa membrane, assuring that changes in molecular size resulting from changes in ionic strength could be readily detected. Solutions of TMK NOM (10 mg l^{-1}, pH 7) were prepared with a range of ionic strengths varying from 0.01 to 0.1 M as NaCl. Fig. 7 illustrates a decrease in NOM rejection by the UF membrane from 0.44 to 0.12 with an increase in ionic strength from 0.01 to 0.10 M. One explanation for the observed decrease in rejection is that NaCl screened charge on the UF membrane pore walls, reducing charge repulsion. This explanation was ruled out because ionic strength had no effect of the flux of NaCl solutions (data not shown), suggesting the membrane surface charge was small, consistent with manufacturer data. Therefore, we interpret the decrease in rejection with increasing ionic strength as evidence of a more compact NOM configuration (possibly becoming more a rigid, coiled, and spherical) with increasing ionic strength. This conclusion is supported by the data shown in Fig. 8, illustrating that the weight-averaged molecular weight of NOM components permeating the UF membrane (measured using size exclusion chromatography) is significantly higher for the feed having an ionic strength of 0.10 M as compared to 0.01 M. Therefore, the observed increases in specific resistance of the cake formed during filtration are attributed to a reduced cake porosity resulting from a reduction in NOM size or size distribution, and hence a more densely compacted NOM layer. It appears that the specific resistance approaches a limiting value as the reduction in NOM size also reaches a limiting value at ionic strengths ranging from 0.08 to 0.10.

Fig. 9 combines selected flux data from Figs. 3 and 6 to illustrate the contributions of salt concentration polarization and NOM cake formation on solution flux. Data correspond-

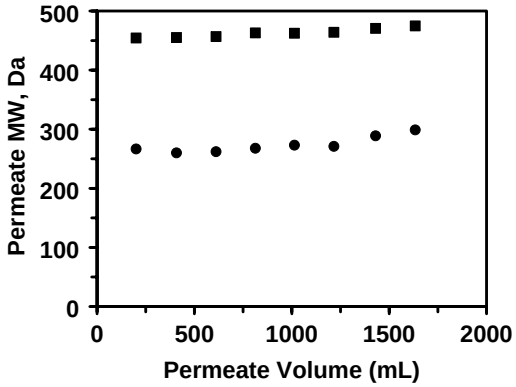

Fig. 8. The effect of ionic strength on the molecular weight of NOM components permeating through a 5 kDa UF membrane. NOM concentration = 10 mg l^{-1}, pH = 7. Ionic strength: (■) 0.1 M NaCl, (●) 0.01 M NaCl. Operating conditions: transmembrane pressure 10 psi, and temperature = 23 °C.

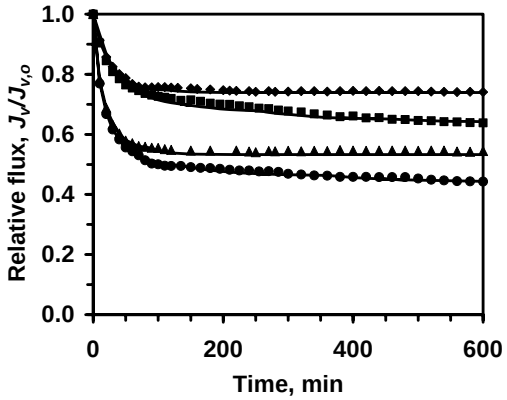

Fig. 9. Comparison solution flux reduction due to salt concentration polarization and NOM cake formation at two ionic strengths. Symbols show experimental data while the solid lines are model fits. Feed solutions: (◆) 0.01 M NaCl, NOM-free; (■) 0.01 M NaCl, 10 mg l^{-1} TMK NOM; (▲) 0.05 M NaCl, NOM-free; (●) 0.05 M NaCl, 10 mg l^{-1} TMK NOM. All solutions pH 7. Operating conditions: initial solution flux = 1.25×10^{-5} m s^{-1}, crossflow velocity = 0.1 m s^{-1}, recovery = 0.85, and temperature = 23 °C.

ing to ionic strengths of 0.01 and 0.05 M are shown. As is apparent from the data, in both cases the initial rates of permeate flux decline were caused primarily by salt concentration polarization and NF membrane permeability reduction. In

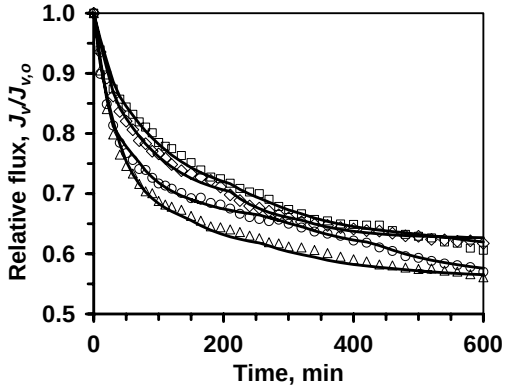

Fig. 10. Effect of pH on NOM solution flux. Symbols show experimental data while the solid lines are model fits. NOM concentration = 14 mg l^{-1}, ionic strength = 0.01 M NaCl. pH values: (◇) pH 3; (□) pH 4 (pH ≈ pI); (△) pH 7; (○) pH 10. Operating conditions: initial solution flux = 1.25×10^{-5} m s^{-1}, crossflow velocity = 0.1 m s^{-1}, recovery = 0.85, and temperature = 23 °C.

the absence of NOM, the solution flux reached a steady-state condition (i.e. $C_{reten,s}$ was constant) after the first hour of filtration. In the presence of NOM, the solution flux decreased with time over the entire operating period, consistent with a NOM cake formation mechanism. The absolute reduction in solution flux relative to the NOM-free experiment was quite similar for the two ionic strengths. However, because the solution flux for the high ionic strength run was significantly lower, a smaller amount of mass was transported to the membrane surface. To result in the same flux reduction as compared to the low ionic strength run, the cake layer formed must have had a greater resistance to solution flux. This is quantified by the specific resistance (Table 6), which increased by about 50%.

4.7. Effect of pH in the presence of NOM

Fig. 10 illustrates the effect of pH on solution flux. The solid lines represent model fits to Eq. (6); directly measured process parameters and fitted model parameters are tabulated in Table 7. For these experiments, a separate batch of concentrated TMK–NOM was diluted to 14 mg l^{-1} DOC and ionic strength was adjusted to 0.01 M as NaCl. After 10-h

Table 7
Model and process performance parameters, TMK–NOM feed, effect of pH

pH	J/J_0 (10 h)	α_{cake} (m/kg) $\times 10^{-16}$[a]	J^* (LMH)[b]	$\mathcal{R}_{feed}$ %DOC[c]	$\mathcal{R}_{feed}$ %conductivity[c]
3	0.617	2.32	28.5	86.4–87.4 (87.1)	21.0–27.9 (25.5)
4	0.606	2.15	27.8	79.6–81.8 (80.2)	21.0–23.8 (22.1)
7	0.561	2.38	25.6	92.6–93.5 (93.0)	46.1–56.7 (49.5)
10	0.570	1.29	25.8	84.1–85.3 (84.1)	33.9–40.9 (36.6)

Solution conditions: NOM concentration: 14 mg l^{-1}; ionic strength: 0.01 M as NaCl. Operating conditions: initial solution flux = 1.25×10^{-5} m s^{-1}, crossflow velocity = 0.1 m s^{-1}, recovery = 0.85, temperature = 23 °C. The average of seven rejection values is shown in the parenthesis.

[a] The specific cake resistance, α_{cake}, was determined with an approximate 95% confidence interval within ±10% of the stated value.

[b] The effective back transport flux, J^*, was determined with an approximate 95% confidence interval within ±2% of the stated value.

[c] $\mathcal{R}_{feed} = 1 - C_{perm}/C_{feed}$; C_{perm} and C_{feed} are the permeate and feed reservoir DOC concentrations or conductivities, respectively.

Table 8
Process performance parameters, effect of $CaCl_2$ concentration

$CaCl_2$ (M)	NaCl (M)	NOM[a] ($mg\,l^{-1}$)	J/J_0 (10 h)	$\mathcal{R}_{feed}$ (%Ca^{2+})[a]	$\mathcal{R}_{feed}$ (%Na^{+})[a]	$\mathcal{R}_{feed}$ (%conductivity)[a]	$\mathcal{R}_{feed}$[a] (%DOC)[b]
0.0	0.01	0.0	0.74	–	ND	45–51 (46)	–
0.0	0.01	10	0.64	–	ND	70–80 (73)	(98)
0.001	0.007	0.0	0.81	64–71 (68)	30–42 (37)	42–46 (43)	–
0.001	0.007	10	0.61	87–94 (91)	63–79 (72)	62–67 (64)	(95)

Solution conditions: ionic strength = 0.01; pH 7. Operating conditions: initial solution flux = $1.25 \times 10^{-5}\,m\,s^{-1}$, crossflow velocity = $0.1\,m\,s^{-1}$, recovery = 0.85, temperature = 23 °C. The average of seven rejection values is shown in parenthesis. ND: not determined.

[a] $\mathcal{R}_{feed} = 1 - C_{perm}/C_{feed}$; C_{perm} and C_{feed} are the permeate and feed reservoir concentrations of the species indicated, respectively.

[b] Rejection values varied over a range less than 1% of stated value.

filtration, the normalized solution flux of pH 3, 4, 7, and 10 were approximately 0.62, 0.61, 0.56, and 0.57, respectively. These results show a reduced effect of pH in the presence of NOM as compared with results obtained in the absence of NOM. Surprisingly, the lowest pH values (3 and 4) exhibited somewhat less fouling than the higher pH values; at low pH, NOM molecules are more protonated, and a greater fouling potential would be expected. However, negative charge on the membrane is also more effectively screened; Vrijenhoek et al. [44] report that the NF-70 membrane carries a small positive charge at pH 3 (∼3 mV) and a small negative charge (∼−8 mV) at pH 4. Therefore, salt rejection is low as compared to higher pH values, and overall flux decline is less severe. As the pH increases, NOM functional groups become ionized, membrane charge becomes more negative, and membrane permeability increases (i.e., η approaches unity). At pH 7 specific cake resistance is statistically similar to the lower pH values, however, the increase in salt rejection becomes significant; therefore, flux decline is most severe at this pH. As the pH increases further to 10, the reduction in specific cake resistance is statistically significant, and salt rejection declines somewhat. These factors combine to reduce the magnitude of flux decline. The reduction in cake resistance is expected, based on ionization of, and charge repulsion between, NOM functional groups within the cake. A decrease in rejection at pH values above 8 was not expected, but similar behavior has been observed previously for the FT-30 membrane [59]. It is possible that the reduction observed here was related to the increase in membrane permeability.

4.8. Effect of calcium on NOM fouling

Multivalent cations (calcium) have been shown to significantly affect membrane fouling [2,15,24]. Process performance parameters for several runs in the presence of $CaCl_2$ are tabulated in Table 8; these are compared to parameters determined in the absence of $CaCl_2$ (reported above). Calcium has the ability to interact strongly with weak acid groups in the membrane phase, thus reducing fixed charge density [26]. Such a reduction in charge density would be expected to reduce membrane permeability, potentially increasing flux decline. However, in the absence of NOM, flux decline caused by a feed solution of NaCl was more pronounced ($J/J_0 = 0.74$) than the decline caused by a solution composed of NaCl and $CaCl_2$ ($J/J_0 = 0.81$) having the same ionic strength. The ability of calcium to mitigate flux decline appears to be related primarily to a reduction in osmotic pressure. The major effect seems to be related to the significant reduction in sodium rejection observed when calcium was present. In addition, the ideal osmotic pressure of the solution containing calcium is about 15% lower than the 0.01 M NaCl solution. A minor effect (on the order of a few percent over the concentration range studied here) may be related to the somewhat lower osmotic coefficient exhibited by $CaCl_2$ solutions as compared with NaCl solutions; e.g., at a concentration of $0.01\,mol\,kg^{-1}$ the molal osmotic pressure coefficient for $CaCl_2$ is 0.908 while that of NaCl is 0.968.

The presence of NOM increased flux decline, reducing J/J_0 from 0.74 to 0.64 in the absence of calcium and from 0.81 to 0.61 in the presence of calcium. Therefore, while the increase was greater, the flux decline caused by NOM fouling in the presence of calcium was only slightly lower than that caused by NOM in a solution of NaCl at the same ionic strength. Flux decline caused by NOM in the absence of calcium was caused, in part, by a significantly increased rejection of NaCl; in the presence of calcium, the rejection of conductivity was lower. In addition, as discussed above, the feed osmotic pressure is lower in the presence of calcium at constant ionic strength. However, it is likely that calcium is more effective at reducing charge repulsion between ionized functional groups on NOM molecules, as a result of complex or ion pair formation, with subsequent lowering of cake porosity (an increase of cake resistance) through decreased electrostatic repulsion or increased cross-linking [15]. Significant binding of calcium by TMK NOM is shown in Fig. 11. As is evident from the data shown in this figure, a total calcium concentration of 0.001 M was not sufficient to saturate calcium binding sites on the NOM; therefore, a low free calcium ion concentration is expected. This is consistent with the significant increase in calcium rejection observed in the presence of NOM, from 68 to 91%, likely as a result of binding by NOM. The similar flux decline caused by NOM in the presence and absence of calcium at constant ionic strength suggests that the tendency of calcium binding to reduce ion rejection by NOM is balanced by an increase in NOM cake resistance.

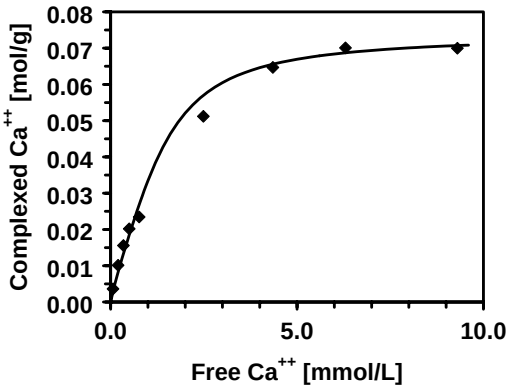

Fig. 11. Calcium uptake by TMK NOM. NOM concentration = 10 mg l^{-1}; pH 7. Line indicates parametric trend.

To examine the effect of calcium in more detail, the calcium concentration was varied over a wide range; the resulting flux decline is shown in Fig. 12. Process performance parameters are tabulated in Table 9. In these experiments the TMK NOM was employed at a concentration of 8.5 mg l^{-1}. Because high calcium concentrations were investigated, a baseline ionic strength of 0.05 M (NaCl + $CaCl_2$) was used. Consistent with the findings discussed above, flux decline caused by NOM fouling in the presence of calcium was similar to that caused by NOM in a solution of NaCl at the same ionic strength, up to a calcium concentration of 0.01 M. However, there was a significant effect at a calcium concentration of 0.015 M; the normalized solution flux decreased to 0.39 from about 0.58. Based on the binding isotherm shown in Fig. 11, it is evident that calcium uptake reached a maximum at a total calcium concentration of 0.0075 to 0.01 M $CaCl_2$. Therefore, it appears that calcium exerted a significant effect only after the binding sites on the NOM became

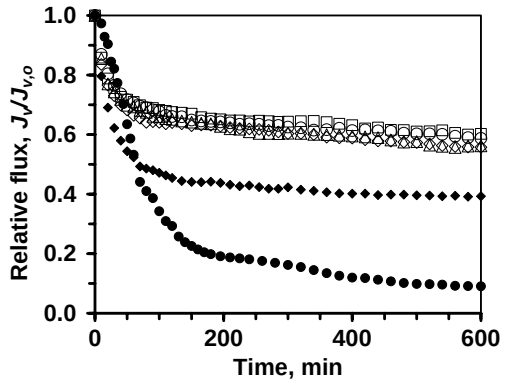

Fig. 12. Effect of calcium concentration, at constant ionic strength, on normalized solution flux. Solutions without phosphate: NOM concentration = 8.5 mg l^{-1}; ionic strength = 0.05 M (NaCl + $CaCl_2$); pH 7. Calcium concentrations: (◇) 0.0 M $CaCl_2$; (□) 0.001 M $CaCl_2$; (△) 0.005 M $CaCl_2$; (○) 0.01 M $CaCl_2$; (◆) 0.015 M $CaCl_2$. Solution with 1×10^{-3} M phosphate (●): NOM concentration = 10 mg l^{-1}; ionic strength = 0.01 M (NaCl + 0.001 M $CaCl_2$); pH 7. Operating conditions: initial solution flux = 1.25×10^{-5} m s^{-1}, crossflow velocity = 0.1 m s^{-1}, recovery = 0.85, and temperature = 23 °C.

Table 9
Process performance parameters TMK–NOM feed, effect of $CaCl_2$ concentration

$CaCl_2$ (M)	J/J_0 (10 h)	$\mathcal{R}_{feed}$ (%DOC)[a]	$\mathcal{R}_{feed}$ (%conductivity)[a]
0.00[b]	0.56	95.7–96.5 (96.1)	27.0–29.2 (28.0)
0.001[b]	0.60	95.0–96.1 (95.5)	25.5–27.8 (26.4)
0.005[b]	0.56	90.3–91.2 (90.7)	26.5–29.5 (27.4)
0.010[b]	0.59	85.8–88.2 (86.9)	24.5–26.5 (25.3)
0.015[b]	0.39	93.2–95.0 (93.7)	39.9–49.1 (42.3)
0.001[c]	0.09	93.6–96.5 (95.1)	36.7–73.0 (51.1)

Operating conditions: initial solution flux = 1.25×10^{-5} m s^{-1}, crossflow velocity = 0.1 m s^{-1}, recovery = 0.85, temperature = 23 °C. The average of seven rejection values is shown in parenthesis.

[a] $\mathcal{R}_{feed} = 1 - C_{perm}/C_{feed}$; C_{perm} and C_{feed} are the permeate and feed reservoir DOC concentrations or conductivities, respectively.

[b] NOM concentration = 8.5 mg l^{-1}, ionic strength = 0.05 M (NaCl + $CaCl_2$); pH 7.

[c] NOM concentration = 10 mg l^{-1}, ionic strength = 0.05 M (NaCl + $CaCl_2$); pH 7; $HPO_4^{2-} + H_2PO_4^- = 1 \times 10^{-3}$ M (added as sodium salt).

saturated. As discussed by Hong and Elimelech [15], part of the flux decline is likely related to the ability of calcium to reduce NOM charge density, reduce electrostatic repulsion between humic macromolecules, and thus create a denser NOM cake on the membrane surface.

The effect of calcium in the presence of 0.001-M phosphate buffer ($HPO_4^{2-} + H_2PO_4^- = 1 \times 10^{-3}$ M) is also shown in Fig. 12. Significant flux decline due to fouling was observed during this experiment, despite a low calcium concentration of 0.001 M $CaCl_2$ (I.S. = 0.01 M). Equilibrium calculations suggest the likelihood that the solution was unstable (oversaturated) with respect to a hydroxyapatite solid phase. While direct measurements were not made, it is possible that the formation of such an inorganic precipitate formation caused the extensive flux decline observed, which was significantly different from the flux decline caused by NOM cake formation. It was also observed that the conductivity rejection decreased significantly from 73 to 39% during filtration. This is consistent with the effect of calcium in the absence of NOM. One explanation for this observation is that the precipitate was involved in the co-adsorption or complexation of NOM, reducing its ability to enhance salt rejection by charge repulsion.

5. Conclusions

Feed solution chemistry and natural organic matter influenced flux decline during nanofiltration using a negatively charged aromatic polyamide membrane. The effects of solution chemistry on solute and solution flux were modeled conceptually in terms of the effects of ions shielding charge on the membrane surface. For the negatively charged membrane studied here, shielding occurred at low pH and high ionic strength; small amounts of calcium were also effective. When membrane charge was neutralized or shielded

the membrane permeability was reduced, possibly due to a reduction in membrane porosity or pore size. Solute rejection was also reduced, consistent with Donnan exclusion. Both mechanisms can have a significant effect on solution flux. Flux decline was modeled by accounting for changes in osmotic pressure with time, and by employing an effective permeability. With increasing ionic strength, the dominant mechanism was a reduction in effective permeability. With increasing pH (at constant ionic strength), the effective permeability increased, but solution flux still decreased as a result of increased osmotic effects resulting from increased solute rejection. This behavior is in contrast to looser membranes having low salt rejection, for which solution flux increases with increasing pH as a result of increases in membrane permeability.

The presence of NOM caused greater flux decline resulting from a combination of NOM cake resistance and increased rejection of NaCl by negatively charged NOM functional groups. Increasing NaCl concentration had little effect on the mass of NOM deposited, but significantly increased the specific resistance of the NOM cake. The effect of ionic strength on specific resistance correlated with a reduction in NOM size, estimated by separate UF permeation experiments and size exclusion chromatography analysis of UF permeate. Therefore, increased specific cake resistance is consistent with a more compact, less porous cake. Flux decline by NOM solutions showed a maximum at pH 7, where salt rejection was also a maximum. Flux decline caused by NOM fouling in the presence of calcium was only significantly different than that caused by NOM in a solution of NaCl at the same ionic strength when the calcium concentration corresponded to saturation of NOM binding sites.

Acknowledgements

This research was supported by the US Department of the Interior, Bureau of Reclamation, Desalination Research and Development Program (Grant 98-FC-81-0061); the National Science Foundation, Division of Chemical and Thermal Systems (Grant CTS-9400610) and Division of Bioengineering and Environmental Systems (Grants BES-9871241 and BES-9984709); and the US Department of Energy, Basic Chemical Sciences Division (Grant #DE-FG02-90ER14114). No agency review was done, and no official endorsement should be inferred. J.E. Kilduff also gratefully acknowledges support from the Eastman Kodak Company.

References

[1] AWWA membrane technology research committee, membrane processes in potable water treatment, J. AWWA 84 (1992) 59–67.
[2] A.I. Schafer, A.G. Fane, T.D. Waite, Nanofiltration of natural organic matter: removal, fouling and the influence of multivalent ions, Desalination 118 (1998) 109–122.
[3] J.S. Taylor, D.M. Thompson, J.K. Carswell, Applying membrane processes to groundwater sources for trihalomethane precursor control, J. AWWA 79 (8) (1987) 72–82.
[4] T.J. Blau, J.S. Taylor, K.E. Morris, L.A. Mulford, DBP control by nanofiltration: cost and performance, J. AWWA 84 (1992) 104–116.
[5] P. Fu, H. Ruiz, K. Thompson, C. Spangenberg, Selecting membranes for removing NOM and DBP precursors, J. AWWA 86 (1994) 55–72.
[6] P. Eriksson, Nanofiltration extends the range of membrane filtration, Environ. Prog. 7 (1) (1988) 58–62.
[7] B.M. Watson, C.D. Hornburg, Low-energy membrane nanofiltration for removal of color, organics and hardness from drinking water supplies, Desalination 72 (1989) 11–22.
[8] S.J. Duranceau, J.S. Taylor, L.A. Mulford, SOC removal in a membrane softening process, J. AWWA 84 (1) (1992) 68–78.
[9] R.J. Petersen, Composite reverse osmosis and nanofiltration membranes, J. Membr. Sci. 83 (1993) 81–150.
[10] M. Kabsch-Korbutowicz, G. Pozniak, W. Trochimczuk, T. Winnicki, Separation of humic substances by porous ion-exchange membranes from sulfonated polysulfone, Sep. Sci. Technol. 29 (1994) 2345–2358.
[11] Y. Kaiya, Y. Itoh, K. Fujita, S. Takizawa, Study on fouling materials in the membrane treatment process for potable water, Desalination 106 (1996) 71–77.
[12] W. Yuan, A.L. Zydney, Humic acid fouling during microfiltration, J. Membr. Sci. 157 (1999) 1–12.
[13] J.A. Nilson, F.A. DiGiano, Influence of NOM composition on nanofiltration, J. AWWA 88 (5) (1996) 53–66.
[14] A. Braghetta, F.A. DiGiano, W.P. Ball, Nanofiltration of natural organic matter: pH and ionic strength effects, J. Environ. Eng., ASCE 123 (1997) 628–641.
[15] S. Hong, M. Elimelech, Chemical and physical aspects of natural organic matter (NOM) fouling of nanofiltration membranes, J. Membr. Sci. 132 (1997) 159–181.
[16] J. Cho, G.L. Amy, J. Pellegrino, Membrane filtration of natural organic matter: initial comparison of rejection and flux decline characteristics with ultrafiltration and nanofiltration membranes, Water Res. 33 (1999) 2517–2526.
[17] C. Combe, E. Molis, P. Lucas, R. Riley, M.M. Clark, The effect of ca membrane properties on adsorptive fouling by humic acid, J. Membr. Sci. 154 (1999) 73–87.
[18] M. Manttari, L. Purom, J. Nuortila-Jokinen, M. Nystrom, Fouling effects of polysaccharides and humic acid in nanofiltration, J. Membr. Sci. 165 (2000) 1–17.
[19] J.E. Kilduff, S. Mattaraj, J. Sensibaugh, J.P. Pieracci, Y. Yuan, G. Modeling, Flux decline during nanofiltraiton of nom with poly-(arylsulfone) nanofiltration membranes modified using UV-assisted graft polymerization, Environ. Eng. Sci. 19 (6) (2002) 477–496.
[20] C. Jucker, M.M. Clark, Adsorption of aquatic humic substances on hydrophobic ultrafiltration membranes, J. Membr. Sci. 97 (1994) 37–52.
[21] K.L. Jones, C.R. O'Melia, Protein and humic acid adsorption onto hydrophilic membrane surfaces: effects of pH and ionic strength, J. Membr. Sci. 165 (2000) 31–46.
[22] A. Braghetta, F.A. DiGiano, W.P. Ball, NOM accumulation at nf membrane surface: impact of chemistry and shear, J. Environ. Eng., ASCE 124 (11) (1998) 1087–1098.
[23] P. Bacchin, P. Aimar, V. Sanchez, Influence of surface interaction on transfer during colloid ultrafiltration, J. Membr. Sci. 115 (1996) 49–63.
[24] S.-H. Yoon, C.-H. Lee, K.-J. Kim, A.G. Fane, Effect of calcium ion on the fouling of nanofilter by humic acid in drinking water production, Water Res. 32 (1998) 2180–2186.
[25] W. Yuan, A.W. Zydney, Humic acid fouling during ultrafiltration, Environ. Sci. Technol. 34 (2000) 5043–5050.
[26] A. Yaroshchuk, E. Staude, Charged membranes for low pressure reverse osmosis properties and applications, Desalination 86 (1992) 115–134.

[27] P. Eriksson, Water and salt transport through two types of polyamide composite membranes, J. Membr. Sci. 36 (1988) 297–313.
[28] A.J. Van Reenen, R.D. Sanderson, Dynamically formed hydrous zirconium (IV) oxide-polyelectrolyte membranes. VII. Poly(acrylic acid-co-vinyl acetate) and poly(acrylic acid-co-vinyl alcohol) membranes: the effect of feed salt concentration on membrane properties, Desalination 85 (1992) 247–262.
[29] S.M. Serkiz, E.M. Perdue, Isolation of dissolved organic matter from the suwannee river using reverse osmosis, Water Res. 24 (7) (1990) 911–916.
[30] L. Sun, E.M. Perdue, J.F. McCarthy, Using reverse osmosis to obtain organic matter from surface and ground waters, Water Res. 29 (1995) 1471–1477.
[31] Y.-P. Chin, G. Aiken, E. O'Loughlin, Molecular weight, polydispersity, and spectroscopic properties of aquatic humic substances, Environ. Sci. Technol. 28 (1994) 1853–1858.
[32] J.E. Kilduff, T. Karanfil, Y.P. Chin, W.J. Weber Jr., Adsorption of natural organic polyelectrolytes on activated carbon: a size exclusion chromatography study, Environ. Sci. Technol. 30 (1996) 1336–1343.
[33] E.M. Thurman, G.R. Aiken, R.L. Malcolm, Prediction of capacity factors for aqueous organic solutes adsorbed on a porous acrylic resin, Anal. Chem. 50 (1978) 775.
[34] E.M. Thurman, Organic Geochemistry of Natural Waters, Martinus Nijhoff/Dr. W. Junk Publishers, Dordrecht, The Netherlands, 1985.
[35] R.F. Mantoura, J.P. Riley, The analytical concentration of humic substances from natural waters, Anal. Chim. Acta 76 (1975) 97–106.
[36] G.R. Aiken, E.M. Thurman, R.L. Malcolm, H.F. Walton, Comparison of XAD macroporous resins for the concentration of fulvic acid from aqueous solution, Anal. Chem. 51 (1979) 1799.
[37] J.A. Leenheer, Comprehensive approach to the preparative isolation and fractionation of dissolved organic carbon from natural waters and wastewaters, Environ. Sci. Technol. 15 (1981) 578.
[38] E.M. Thurman, R.L. Malcolm, Preparative isolation of aquatic humic substances, Environ. Sci. Technol. 15 (1981) 463.
[39] M.R. Collins, G.L. Amy, C. Steelink, Molecular weight distribution, carboxylic acidity, and humic substances content of aquatic organic matter: implications for removal during water treatment, Environ. Sci. Technol. 20 (1986) 1028–1032.
[40] G. Newcombe, M. Drikas, S. Assemi, R. Beckett, Influence of characterized natural organic material on activated carbon adsorption. I. Characterization of concentrated reservoir water, Water Res. 31 (1997) 965–972.
[41] J.J. McCreary, V.L. Snoeyink, Characterization and activated carbon adsorption of several humic substances, Water Res. 14 (1980) 151–160.
[42] B.G. Oliver, E.M. Thurman, R.L. Malcolm, The contribution of humic substances to the acidity of colored natural waters, Geochim. Cosmochim. Acta 47 (1983) 2031–2035.
[43] A.E. Childress, M. Elimelech, Effect of solution chemistry on the surface charge of polymeric reverse osmosis and nanofiltration membrane, J. Membr. Sci. 119 (1996) 253–268.
[44] E.M. Vrijenhoek, S. Hong, M. Elimelech, Influence of membrane surface properties on initial rate of colloidal fouling of reverse osmosis and nanofiltration membranes, J. Membr. Sci. 188 (2001) 115–128.
[45] P. Fu, H. Ruiz, J. Lozier, K. Thompson, C. Spangenberg, A pilot study on groundwater natural organics removal by low-pressure membranes, Desalination 102 (1995) 47–56.
[46] S.C. Allgeier, R.S. Summers, Evaluating NF for DBP control with the RBSMT, J. AWWA 87 (3) (1995) 87–99.
[47] A.R. Da Costa, A.G. Fane, D.E. Wiley, Spacer characterization and pressure drop modeling in spacer-filled channels for ultrafiltration, J. Membr. Sci. 87 (1994) 79–98.
[48] A.D. Eaton, L.S. Clesceri, A.E. Greenberg (Eds.), Standard Methods for the Examination of Water and Wastewater, 19th ed., Washington, DC, 1995.
[49] J.E. Kilduff, W.J. Weber Jr., Transport and separation of organic macromolecules in ultrafiltration processes, Environ. Sci. Technol. 26 (1992) 569–577.
[50] B.E. Logan, Q. Jiang, Molecular size determination of dissolved organic matter, J. Environ. Eng. 116 (1990) 1046–1062.
[51] C.J. Geankoplis, Transport Processes and Unit Operations, third ed., Prentice Hall, Eaglewood Cliffs, New Jersey, 1993.
[52] M. Taniguchi, J.E. Kilduff, G. Belfort, Modes of natural organic matter fouling during ultrafiltration, Environ. Sci. Technol. 37 (2003) 1676–1683.
[53] J. Hermia, Constant pressure blocking filtration laws: application to power-law non-Newtonian fluids, Trans. Inst. Chem. Eng. 60 (1982) 183–187.
[54] R.W. Field, D. Wu, J.A. Howell, B.B. Gupta, Critical flux concept for microfiltration fouling, J. Membr. Sci. 100 (1995) 259–272.
[55] L.J. Zeman, A.L. Zydney, Microfiltration and Ultrafiltration: Principles and Applications, M. Dekker, New York, 1996.
[56] A.R. Da Costa, A.G. Fane, C.J.D. Fell, A.C.M. Franken, Optimal channel spacer design for ultrafiltration, J. Membr. Sci. 62 (1991) 275–291.
[57] G. Schock, A. Miguel, Mass transfer loss in spiral wound modules, Desalination 64 (1987) 339–352.
[58] N.S. Pujar, A.L. Zydney, Electrostatic and electrokinetic interactions during protein transport through narrow pore membranes, Ind. Eng. Chem. Res. 33 (1994) 2473–2482.
[59] J.E. Cadotte, R.J. Petersen, R.E. Larson, E.E. Erickson, A new thin film seawater reverse osmosis membrane, Desalination 32 (1980) 25–31.
[60] D.L. Comstock, Desal-5 membrane for water softening, Desalination 76 (1989) 61–72.
[61] M. Schnitzer, Soil organic matter—the next 75 years, Soil Sci. 151 (1991) 41–58.
[62] R.D. Cohen, R.F. Probstein, Colloidal fouling of reverse osmosis membranes, J. Colloid Interface Sci. 114 (1986) 195–207.
[63] K. Ghosh, M. Schnitzer, Macromolecular structures of humic substances, Soil Sci. 129 (1980) 266–276.
[64] P.K. Cornel, R.S. Summers, P.V. Roberts, Diffusion of humic acid in dilute aqueous solution, J. Colloid Interface Sci. 110 (1986) 149–164.